colorants

MDPI

Article

Metal-Free Counter Electrodes for DSSCs Based on Nitrogen-Doped Reduced Graphene Oxide Materials

Isolda Duerto [1], Clara Carrera [2], Daniel Barrios [3], Ana M. Benito [2], Wolfgang K. Maser [2], Belén Villacampa [3], Enrique García-Bordejé [2] and María-Jesús Blesa [1,*]

[1] Departamento de Química Orgánica, INMA, Universidad de Zaragoza-CSIC, 50009 Zaragoza, Spain; isolda@unizar.es
[2] Instituto de Carboquímica, ICB-CSIC, Miguel Luesma Castán 4, 50018 Zaragoza, Spain; ccarrera@icb.csic.es (C.C.); abenito@icb.csic.es (A.M.B.); wmaser@icb.csic.es (W.K.M.); jegarcia@icb.csic.es (E.G.-B.)
[3] Departamento de Física de la Materia Condensada, INMA, Universidad de Zaragoza-CSIC, 50009 Zaragoza, Spain; danielb@unizar.es (D.B.); bvillaca@unizar.es (B.V.)
* Correspondence: mjblesa@unizar.es

Abstract: The importance of counter electrodes in Dye Sensitized Solar Cells (DSSCs) cannot be neglected as they enable the transfer of electrons across the outer circuit, thereby facilitating the reduction reaction of the I_3^-/I^- redox electrolyte. However, the dissolution and deposition of the usual platinum layer on the counter electrode has resulted in contamination concerns. To address this issue, metal-free counter electrodes made of reduced graphene oxide (rGO) aerogels were developed and their catalytic performance towards I_3^- reduction was evaluated. The reduced graphene materials were characterized, and the fitting analysis of XPS revealed the presence of various nitrogen species, with the primary peaks attributed to pyridinic and pyrrolic nitrogen. The hydrothermal treatment of graphene oxide (GO) resulted in a higher graphitic character and the intensification of the contacts between graphene nanosheets, which should entail higher electrical conductivity, both in-plane and between rGO sheets. Additionally, the presence of nitrogen-provided active sites promoted the catalytic reduction of the electrolyte. Encouragingly, good charge transfer rates were observed between the counter electrode and the electrolyte in the assembled DSSCs, resulting in good photocurrents and exceptional stability over the course of nearly 1200 h after cell assembly. The results obtained suggest that these GO-based systems are promising candidates for developing metal-free counter electrodes for DSSC, supporting the interest of further study.

Keywords: graphene; aerogels; dye sensitized solar cells; metal-free counter electrode

Citation: Duerto, I.; Carrera, C.; Barrios, D.; Benito, A.M.; Maser, W.K.; Villacampa, B.; García-Bordejé, E.; Blesa, M.-J. Metal-Free Counter Electrodes for DSSCs Based on Nitrogen-Doped Reduced Graphene Oxide Materials. *Colorants* **2023**, *2*, 443–452. https://doi.org/10.3390/colorants2020020

Academic Editors: Nadia Barbero, Simone Galliano and Carlotta Pontremoli

Received: 4 April 2023
Revised: 1 May 2023
Accepted: 22 May 2023
Published: 16 June 2023

1. Introduction

Dye Sensitized Solar cells (DSSCs) have been considered attractive energy conversion devices because they are easy to build [1]. They are composed of a dye-sensitized semiconductor, which acts as photoanode, a counter electrode and a redox mediator [2]. Here, organic dyes are essential components for sensitizing photoanodes, and their molecular structures play a critical role in this process. These structures can be readily engineered, and they typically exhibit high molar extinction coefficients. Specifically, the donor-π-spacer-acceptor (D-π-A) system is a widely utilized architecture for such dyes. By adequately modulating each constituent (D, π-spacer and A), it is possible to systematically fine-tune the molecular properties and broaden the absorption spectra. This is achieved by adjusting the HOMO and LUMO orbitals to facilitate intramolecular charge separation that, in turn, enhances the dye photovoltaic performance, resulting in improved energy conversion efficiency. The dye is excited upon light absorption, and its efficiency and spectral range are strongly dependent on the nature of D and A subunits, as well as on the π-conjugated bridge that facilitates the intramolecular charge transfer from D to A [3]. The excited dye injects

electrons into the conduction band of the semiconductor through the electron-withdrawing group. Other architectures, like D-A-π-A systems, have been also considered [4]. The low bandgap and the strong electron-withdrawing auxiliary unit of these systems provide favorable properties in the areas of light-harvesting and efficiency for designing efficient and stable organic sensitizers [5,6]. Thus, extensive studies have been conducted to optimize the design of D, π-spacer, and A [7–9] components. Regarding donors, *N*,*N*′-dialkylanilines are interesting due to their intense light absorption, with a red-shifted intramolecular charge transfer band compared to triphenylamines derivatives [10]; π-spacers containing heterocycles, such as thiophenes, are shown to stabilize the sensitizers [11]; and finally, groups such as pyrimidine, with electron withdrawing properties but also acting as an anchoring group, have recently been explored [12].

The DSSC counter electrode (CE) has the function of collecting the flow of electrons from the external circuit and plays an important role because it catalyzes the reduction of the redox couple species (typically I_3^-/I^-, although the use of electrolytes based on other redox couples constitutes an area of growing interest [13]) with the consequent regeneration of the dye. The counter electrode should have a high reduction catalytic activity, low resistance, good stability, and low cost [2]. Numerous assays have been reported with the aim of developing low-cost metal-free catalysts as an alternative to precious metal materials [14]. Carbonaceous materials, such as carbon nanotubes (CNTs) [15] and graphene oxide (GO) [16], possess excellent electrical conductivity, but relatively poor catalytic activity to replace or reduce the use of Pt. Therefore, when attempting to improve device performances with a carbon-based counter electrode, it is crucial to tune the device's electrical conductivity and electrocatalytic activity. In recent years, a variety of metal-free catalysts, such as nitrides, carbides, and oxides, have been proposed to replace Pt. Among these, carbide catalysts have demonstrated higher catalytic activity than Pt for the regeneration of di-5-(1-methyltetrazole)disulfide/5-mercapto-1-methyltetrazole N-tetramethylammonium salt (T_2/T^-) [17]. Furthermore, nitrogen-doped graphene has emerged as a promising metal-free catalyst for DSSCs due to the active sites provided by its nitrogen states, including pyridinic and quaternary nitrogen for the reduction of the electrolyte [18]. In this context, a novel non-catalytic thermal annealing method using melamine has been proposed to prepare nitrogen-doped graphene, which has shown good catalytic activity in alkaline electrolytes, making it a potentially valuable material for DSSC applications [19]. Finally, graphitic carbon has been identified as a viable material for a CE due to its low impact on the working electrode, with CO or CO_2 gases produced as corrosion products easily removable from the counter electrode compartment [20]. Therefore, accurate material characterization, particularly with respect to electrochemical performance, is critical for electrode performance applied to these photovoltaic studies.

This paper aims to explore the performance of carbon counter electrodes based on nitrogen-doped graphene oxide aerogels, while paying attention to the long-term stability of their responses in DSSCs.

2. Materials and Methods

2.1. Preparation of N-Doped Reduced Graphene Oxide Aerogels

The graphene oxide (**GO**) was a commercial 4 mg/mL dispersion from Graphenea Co. (San Sebastián, Spain, Ref. GO-4-1000). The graphene oxide aerogels (**GA**) were prepared according to a previously described procedure [21]. In brief, 10 mL of a 2 mg/mL **GO** aqueous dispersion was mixed with 200 µL of 25% NH_4OH solution and introduced into a Teflon-lined autoclave. The liquid to autoclave volume ratio was 0.22. The autoclave was introduced into an oven at 180 °C, reaching a pressure of 10 bar, and kept for a certain time. We selected two times, namely, 45 min (sample **GA-45 min**) and 18 h (sample **GA-18 h**), separate enough to obtain materials with different properties. Subsequently, the autoclave was withdrawn from the oven and left to cool down at ambient conditions. Likewise, the rate of cooling down was comparable for all the preparations. When the autoclave reached room temperature, it was opened and a monolithic hydrogel was formed.

The hydrogel was introduced into a vial consisting of glass walls and an aluminum bottom. The vial walls are thermally insulated with Styrofoam. The aluminum bottom was placed onto a 5 cm diameter metal platform which was externally cooled by liquid N_2. This created a uniaxial thermal gradient, allowing the hydrogel to cool from the bottom to the top. The solidified cryogel was then transferred into a freeze-drying vessel (Telstar Cryodos) under vacuum (less than 0.3 mbar) and freeze-dried at around 223 K for 48 h to obtain the aerogel. The aerogels were denoted as GA-X, where X is the time of hydrothermal treatment. GO was freeze-dried, and the three materials (**GO**, **GA-45 min** and **GA-18 h**) were ground into powder using a mortar for further characterization or utilization.

The obtained data from the characterization of the GO based materials (ultraviolet visible (UV-vis), scanning electron microscopy (SEM), X-ray diffraction analysis (XRD), X-ray photoelectron spectroscopy (XPS)) can be found in the Supplementary Materials.

2.2. Synthesis and Structural Characterization of the Sensitizer Dye

The dye **AT-Pyri** was the result of the condensation reaction between the aldehyde **AT-CHO** [22] and 4-methylpyrimidine with Aliquat 336 as a phase-transfer catalyst in the alkaline medium [12]. The detailed synthetic procedures (Scheme S1) and spectroscopic data (^{1}H, ^{13}C-NMR spectra, and mass spectrum, Supplementary Materials Figures S1–S5), as well as the corresponding parameters obtained from UV-vis and electrochemical characterization, have already been reported [12].

2.3. DSSC Device Fabrication

Preparation of the counter electrodes: The counter electrodes were prepared using the mentioned **GO**, **GA-45 min** and **GA-18 h** materials.

These aerogels were ground to a powder in an agate mortar; 11 mg of aerogel powder and 3.3 mg of PVPk10 were dispersed into 0.7 mL of ethylene glycol. The paste was maintained for 5 h in an ultrasonic bath. The CEs were made of F-doped tin oxide (FTO) glass (8 Ω·sq-1 sheet resistance). After an ozone treatment of the substrates for 20 min, the three carbonaceous materials were deposited via spin-coating.

The first coating step was conducted at 600 rpm for 9 s, and the second step was conducted at 3600 rpm for 30 s. Finally. these counter electrodes were annealed at 400 °C for 1 h under flowing argon.

Preparation of the photoanodes: Anodes were fabricated by screen printing the TiO_2 paste (Dyesol 18NR-AO) on FTO glass substrates (15 $\Omega \cdot sq^{-1}$ sheet resistance). Prior to the deposition of the TiO_2 paste, the conducting glass substrates were washed sequentially with the cleaning solution Hellmanex III (15 min), MilliQ water (15 min) and ethanol (15 min). The electrodes were heated at 500 °C for 30 min then treated with ozone for 20 min. Finally, they were immersed in a solution of $TiCl_4$ (40 mM) at 90 °C for 30 min, washed with MilliQ water and ethanol and then dried. The screen-printed electrodes were gradually heated up to 325 °C (10 °C/min, 5 min), 375 °C (5 °C/min, 5 min), 450 °C (8 °C/min, 5 min) and 500 °C (5 °C/min, 15 min), and after cooling down these TiO_2 electrodes were immersed again in a solution of $TiCl_4$ (40 mM) at 90 °C for 30 min and then subsequently washed with water and ethanol. The electrodes were heated again at 500 °C for 30 min before the sensitization process. The active area of the devices was 0.25 cm^2.

The TiO_2 photoanodes (7 µm thick) were sensitized with AT-Pyri dye [12] at room temperature by dipping in 0.1 mM dichloromethane dye solution for 72 h. The sensitized electrodes were rinsed with dichloromethane and dried with air.

The *electrolyte* was prepared with 0.53 M 1-butyl-3-methylimidazolium iodide (BMII), 0.1 M lithium iodide, 0.05 M iodine and 0.52 M tert-butylpyridine in anhydrous acetonitrile.

Finally, the photoanode and counter electrodes were sandwiched together using a thin thermoplastic sealing agent (Greatcell) that melts at 120 °C. The cells were prepared in duplicate.

3. Results

3.1. Structural Characterization of the Graphene-Oxide-Based Materials

We studied the effect of the duration of hydrothermal treatment on the dimensions of reduced graphene oxide in a previous article [23]. The external dimensions of the graphene aerogel decreased as the time of hydrothermal treatment increased. This was due to the fact that the graphene sheets intensify their contacts with treatment time, leaving less space between them, as can be observed in Figure S6a,b, corresponding to aerogels **GA-45 min** and **GA-18 h**, respectively.

The characterization of the materials with XRD was also studied previously [21]. The diffractogram of **GO** showed a peak at 2θ = 10°, corresponding to an interlayer spacing of 0.879 nm in agreement with the literature values [24]. This was a consequence of the water intercalation into the space between the graphene layers, as well as of the incorporation of oxygen functional groups (oFGs) in the basal plane during harsh oxidation [25]. For aerogels **GA-18 h** and **GA-45 min,** the peak (002) appeared at 25.1°, which corresponded to an interlayer spacing of around 0.358 nm, which approached natural graphite (0.342 nm). The shorter interlayer spacing compared to **GO** evidenced the intensification of contact between the **rGO** nanosheets after hydrothermal treatment.

The surface chemistry was thoroughly characterized in a previous article by FTIR spectroscopy [23], elemental analysis, TPD and XPS [21]. The quantitative results of these techniques are summarized in Table 1. **GO** contained an O/C ratio = 72.4 wt%, and the oxygen content decreased as the hydrothermal treatment time increased. Unlike **GO**, both aerogels contained up to 6.8 wt.% of nitrogen, which was introduced during the hydrothermal treatment due to NH_4OH being added to the **GO** suspension. The nitrogen content of the aerogels slightly decreased with a longer hydrothermal treatment time. Figure 1 illustrates the fitting of the XPS N 1s peaks for the aerogel materials. The analysis revealed the presence of various nitrogen species, with the primary peaks attributed to pyridinic and pyrrolic nitrogen. The relative contribution of pyridinic nitrogen increased with the progression of hydrothermal treatment. This nitrogen type could act as an active site in the catalytic mechanism of I_3^- reduction.

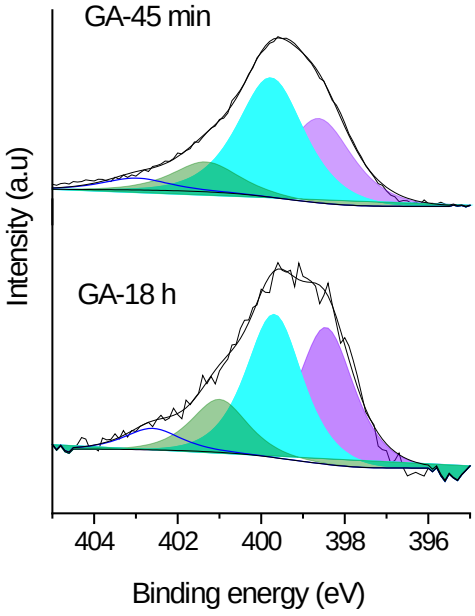

Figure 1. The fitting of N 1s XPS peak (violet: N pyridinic; cyan: N pyrrolic; green: N quaternary; orange: blue: pyridinic oxide).

Table 1. Oxygen and nitrogen content by XPS and elemental analysis [26].

Elemental Analysis		XPS		
O/C	N/C	O/C	N/C	
wt%	wt%	wt%	wt%	
72.4	4.1	n.d	n.d.	**GO**
14.9	10.6	8.9	6.5	**GA-45 min**
13.0	10.3	8.0	6.3	**GA-18 h**

n.d.: Non-determined because it was unstable under the vacuum of the XPS chamber.

3.2. UV-Vis Transmittance Spectra and Electrochemical Characterization of Counter Electrodes

The UV-vis transmittance spectra of the counter electrodes are depicted in Figure S7. The transmittance of **GO** was around 80 % in the range of 600 to 700 nm, while the aerogel counter electrodes exhibited a transmittance of about 60%. The graphitic interlayer distance calculated by XRD ([21], Figure S7) and the space between the thermally reduced **GO** nanosheets (Figure S6) decreased in the order **GO** > **GA-45 min** > **GA-18 h**. The larger distance between the graphene nanosheets for **GO** would favor the transmittance of the light through this material.

In order to evaluate the potential application of the prepared materials as counter electrodes in DSSCs, we conducted Cyclic Voltammetry (CV) to study their electrocatalytic activities. As shown in Figure 2, the left and right peaks at low and high potentials corresponded to I_3^-/I^- and I_2/I_3^-, respectively. As the counter electrode must catalyze the reduction of I_3^- in the electrolyte, we analyzed the peak-to-peak separation (ΔE_p) between oxidation and reduction peaks of the carbonaceous counter electrodes (**GO**, **GA-45 min** and **GA-18 h**). A more effective catalyst was indicated by a reduced ΔE_p. The potential values of the carbonaceous electrodes prepared using the reduced **GO** aerogels (**GA**) were lower than those of **GO**. The wider first oxidation peak observed for **GA 45 min** and **GA-18 h** compared to the **GO** counter electrode indicated that the porous aerogel structure provided a higher number of catalytic reaction sites than the pristine **GO** [15]. Table 1 shows that **GO** had no nitrogen, while **GA-45 min** and **GA-18 h** contained 6–7% nitrogen. The presence of nitrogen in aerogels significantly influenced their catalytic activity because it provided active sites for the reduction of the electrolyte [18]. In addition, the prepared aerogels exhibited higher reduction levels than **GO**, leading to superior electrocatalytic activity for the reduction of the electrolyte. Compared to **GO**, the **GA**-based counter electrodes had lower numbers of oxygen functional groups, resulting in graphene sheets that were more graphitic and had more contacts, consequently leading to graphene materials with increased electrical conductivity both in-plane and between the graphene nanosheets [17].

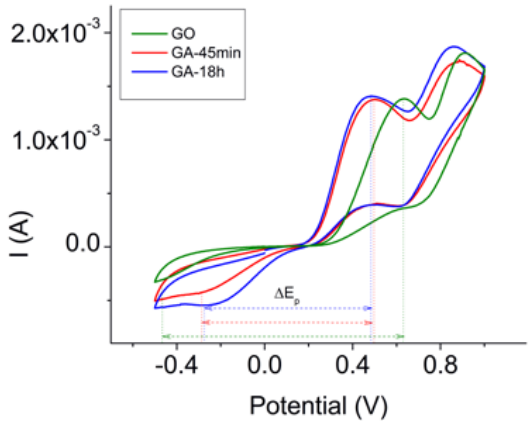

Figure 2. Cyclic voltammograms of counter electrodes of **GO, GA-45 min** and **GA-18 h** versus Ag/AgCl (KCl 3 M), 20 mVs^{-1} scan rate, in the I_3^-/I^- electrolyte (10 mM LiI, 1 mM I_2, 0.1 M $LiClO_4$, Acetonitrile).

3.3. DSSCs Performance

The DSSC device fabrication and its corresponding characterization are described in the Supplementary Materials. The electrolyte was the I_3^-/I^- system in anhydrous acetonitrile [27]. The photoanode was sensitized by **AT-Pyri** (0.1 mM CH_2Cl_2 dye solution) for 72 h. This chromophore was constituted by an aniline as the donor, a thiophene as the π-spacer and a pyrimidine as the anchoring and acceptor group, all this favoring the electron charge transfer towards the semiconductor.

The charge-transfer resistance (*Rct*) at the counter electrode/electrolyte interface is an important parameter for DSSCs power conversion efficiency (PCE), so in order to investigate this phenomenon a study was carried out with electrochemical impedance spectroscopy (EIS).

The electrochemical characteristics were studied in DSSC devices (Figure 3-left). The Nyquist plots in dark conditions and at the open circuit voltage (V_{oc}) of **GO**, **GA-45 min** and **GA-18 h** are shown in Figure 3, on the right.

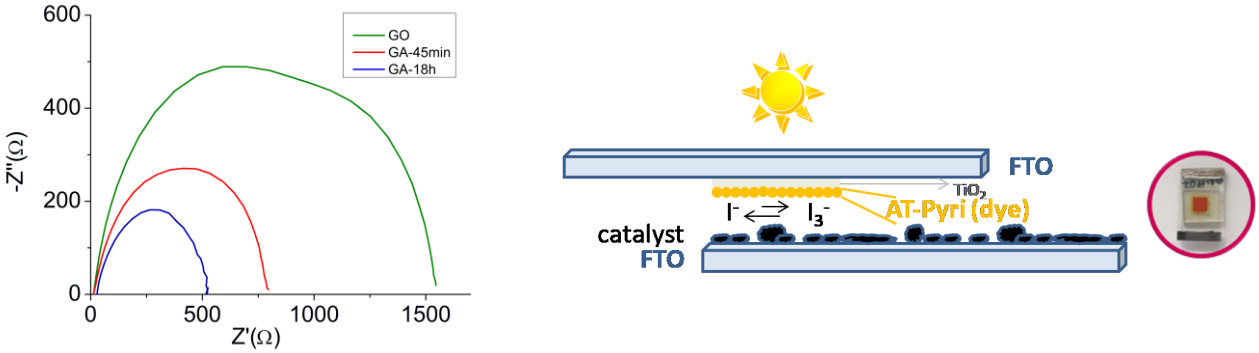

Figure 3. Schematic and photograph of a DSSC device (**left**). Nyquist plot of devices prepared with **GO, GA-45 min** and **GA-18 h** as counter electrode and **AT-Pyri** as dye, 1176 h after assembly. Dark, V_{oc} (**right**).

The Nyquist plots of each carbonaceous electrode cell did not show clearly differentiated arcs, although in some cases more than one contribution could be guessed. The semicircle in the higher frequency range [28] was attributed to the charge-transfer resistance (R_{ct}) at the counter electrode/electrolyte interface, which gave information about the electrocatalytic activity for the reduction of the ion triiodide [29].

The charge-transfer resistance value was small for materials with kinetically fast charge transfer. Then, the R_{CT} value for the counter electrodes decreased in the order of **GO** > **GA-45 min** > **GA-18 h**. The smallest R_{ct} value for **GA-18 h** indicated a faster charge-transfer between the counter electrode and the electrolyte, and hence a superior catalytic effectiveness for the reduction of I_3^- than the **GA-45 min** and **GO** materials. **GA-18 h** showed the smallest *Z*, implying the fast diffusion of the electrolyte to the **GA-18 h** electrode [15].

In order to both simplify and understand the system, symmetrical dummy cells were been built and the Nyquist plots are reported in the Supplementary Materials (Figure S8). This study corroborates the results already obtained (Figure 3, right).

DSSCs are assessed by power conversion efficiency, which is calculated from the current-voltage plots (Figure 4) [30]. The photovoltaic properties of the DSSCs prepared with **GO, GA-45 min** and **GA-18 h** as counter electrode (Table 2), as well as the long-term stability (Table 3) of the characteristic parameters, were evaluated.

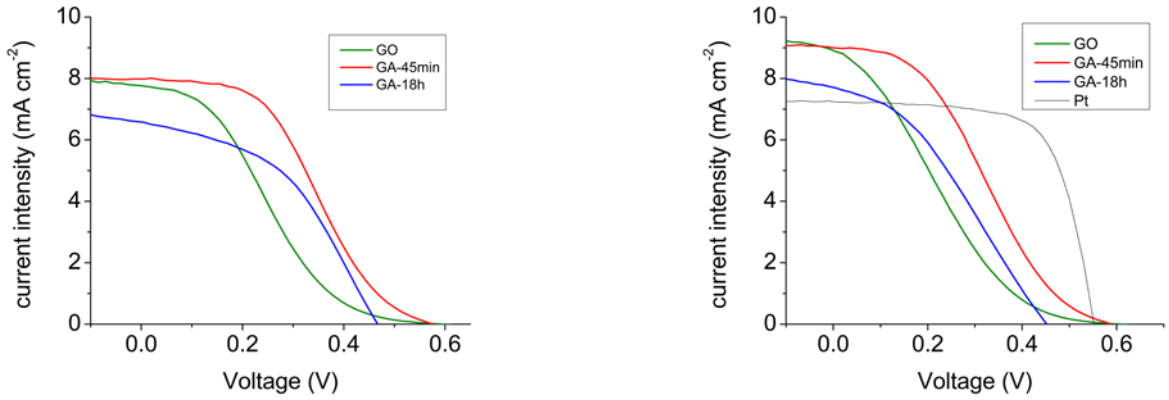

Figure 4. Photocurrent-voltage plots of DSSCs. (**Left**): 24 h after cell assembly; (**right**): 1176 h after cell assembly.

Table 2. Measured photovoltaic parameters of AT-Pyri dye-sensitized solar cells: open circuit voltage (V_{oc}), short circuit current density (J_{sc}), fill factor (*ff*) and overall efficiency (η) at 24 h after cell assembly.

η (%)	*ff* (%)	J_{SC} (mA cm^{-2})	V_{OC} (V)	Catalyst
1.0	18	8.88	0.620	**GO**
1.7	32	9.00	0.590	**GA-45 min**
1.2	35	7.69	0.445	**GA-18 h**
2.7	67	7.23	0.560	**Pt**

Table 3. Measured photovoltaic parameters of AT-Pyri dye-sensitized solar cells: open circuit voltage (V_{oc}), short circuit current density (J_{sc}), fill factor (*ff*) and overall efficiency (η) at 1176 h after cell assembly.

η (%)	*ff* (%)	J_{SC} (mA cm^{-2})	V_{OC} (V)	Catalyst
1.1	23	7.76	0.605	**GO**
1.8	39	7.98	0.575	**GA-45 min**
1.4	45	6.57	0.470	**GA-18 h**

An analogous device was prepared using a Pt counter electrode with the aim of comparing its behavior with these carbonaceous materials. The J/V plots showed the S-shape plots for devices prepared with carbonaceous materials; however, a rectangular response was obtained for the device prepared with platinum as a counter electrode, which may indicate contact problems of carbonaceous materials in these devices [31]. The **GO**-based DSSC exhibited a low power conversion efficiency (PCE) of 1%, primarily attributed to its low fill factor. Interestingly, when carbon materials were used as counter electrodes, the resulting short circuit current density (J_{SC}) was higher than that achieved with platinum as CE. Moreover, a device prepared with **GA-45 min** as the counter electrode displayed a 20% higher J_{SC} than platinum DSSC. This observation could be attributed to the ability of graphene sheets to enhance the electron transport [32].

In the area of DSSCs, the charge transfer resistance (R_{ct}), as measured by *EIS*, was frequently used to elucidate the dissimilarities in the performance of DSSCs employing different counter electrodes. The data presented in Figure 3 demonstrate that a lower R_{ct} value corresponded to a reduced total internal resistance. This is beneficial for improving

the fill factor [18], as indicated in Table 2, particularly in the case of DSSCs fabricated with aerogel **GA-18 h**.

A desirable catalyst should present a high catalytic activity and a good temporal stability. The fill factor improved, but the short circuit current density decreased [33,34]. Accordingly, the performance of the devices was assessed over a period of 1176 h after cell assembly, and the results are shown in Table 3. A comparison with the results obtained from Table 2 revealed an improvement in the fill factor over time. Notably, DSSCs prepared with **GO, GA-45 min** or **GA-18 h** as counter electrodes demonstrated exceptional stability over the course of nearly 1200 h after cell assembly. Previous studies [12] have shown that analogous devices with platinum as counter electrodes have also shown stability over the course of nearly 1000 h.

To sum up, the high interplanar distance in graphene oxide was reduced with hydrothermal treatment, resulting in **rGO** aerogels with higher out of plane conductivity [16]. Meanwhile, the hydrothermal treatment also increased the graphitic character of the graphene sheets in rGO aerogels, which led to superior in-plane conductivity (Figure S6). Moreover, aerogel **GA-45 min** had a higher concentration of oxygen and nitrogen than aerogel **GA-18 h** (Table 1), indicating a higher number of active sites for catalysis. This was consistent with the superior catalytic performance of **GA-45 min** towards electrolyte I_3^- reduction, as well as its better photovoltaic response (Figures 2 and 4 and Tables 2 and 3). This should be confirmed in future works by systematically varying the N content. Notably, an adequate charge transfer rate between the counter electrodes and the electrolyte has also been observed, evidencing sufficient conductivity to prepare devices and showing a higher photocurrent than those using platinum-counter electrodes (Table 2). Additionally, DSSCs incorporating **GO, GA-45 min** or **GA-18 h** as counter electrodes demonstrated high stability for almost 1200 h after cell assembly, with an improvement in the fill factor (Table 3). These promising findings encourage further investigation to develop free-metal counter electrodes for DSSCs.

Supplementary Materials: The following supporting information can be downloaded at: https://www.mdpi.com/article/10.3390/colorants2020020/s1, Figure S1: ^{1}H-NMR spectrum of the dye AT-Pyri ($CDCl_3$); Figure S2: COSY ^{1}H-^{1}H spectrum of the dye AT-Pyri; Figure S3: ^{13}C-NMR spectrum of the dye AT-Pyri ($CDCl_3$); Figure S4: HSQC ^{1}H ^{13}C spectrum of the dye AT-Pyri; Figure S5: Mass spectrum HRMS (ESI^+) of the dye AT-Pyri; Figure S6: SEM characterization: (a) SEM microphotography of GA-45 min; (b) SEM microphotography of GA-18 h; Figure S7: UV spectra of GO, GA-45 min and GA-18 h films (3.1 μm); Figure S8: EIS spectra of dummy cell of GO, GA-45 min and GA-18 h materials; Scheme S1: Preparation of compound AT-Pyri.

Author Contributions: Conceptualization, E.G.-B. and M.-J.B.; Data curation, I.D. and C.C.; Formal analysis, B.V.; Funding acquisition, A.M.B., W.K.M. and B.V.; Investigation, I.D., C.C. and D.B.; Methodology, B.V. and M.-J.B.; Supervision, E.G.-B.; Validation, B.V.; Visualization, E.G.-B. and M.-J.B.; Writing—original draft, E.G.-B. and M.-J.B.; Writing—review and editing, A.M.B., W.K.M., B.V., E.G.-B. and M.-J.B. All authors have read and agreed to the published version of the manuscript.

Funding: We gratefully acknowledge financial support from the Spanish Ministry of Science and Innovation (MICINN) and the Spanish Research Agency (AEI) under projects: PID2019-104307GB-I00/AEI/10.13039/501100011033; PID2019-104272RB-C51/AEI/10.13039/501100011033 and Gobierno de Aragón-Fondo Social Europeo (E47_23R, T03_23R). I.D. and D.B. acknowledge the financial support of the Gobierno de Aragón-Fondo Social Europeo fellowship and PhD studentship Santander-2018 programs, respectively. Finally, C.C. is grateful for her PhD grant from Gobierno de Aragón (DGA).

Institutional Review Board Statement: Not applicable.

Informed Consent Statement: Not applicable.

Data Availability Statement: Not applicable.

Conflicts of Interest: The authors declare no conflict of interest.

References

1. O'Regan, B.; Grätzel, M. A low-cost, high-efficiency solar cell based on dye-sensitized colloidal TiO_2 films. *Nature* **1991**, *353*, 737–740. [CrossRef]
2. Hagfeldt, A.; Boschloo, G.; Sun, L.; Kloo, L.; Pettersson, H. Dye-Sensitized Solar Cells. *Chem. Rev.* **2010**, *110*, 6595–6663. [CrossRef]
3. Yao, Z.; Guo, Y.; Wang, L.; Hao, Y.; Guo, Y.; Franchi, D.; Zhang, F.; Kloo, L.; Sun, L. Energy-Loss Reduction as a Strategy to Improve the Efficiency of Dye-Sensitized Solar Cells. *Sol. RRL* **2019**, *3*, 1900253. [CrossRef]
4. Zhu, W.; Wu, Y.; Wang, S.; Li, W.; Li, X.; Chen, J.; Wang, Z.-S.; Tian, H. Organic D-A-π-A Solar Cell Sensitizers with Improved Stability and Spectral Response. *Adv. Funct. Mater.* **2011**, *21*, 756–763. [CrossRef]
5. Wu, Y.; Zhu, W.-H.; Zakeeruddin, S.M.; Grätzel, M. Insight into D–A−π–A Structured Sensitizers: A Promising Route to Highly Efficient and Stable Dye-Sensitized Solar Cells. *ACS Appl. Mater. Interfaces* **2015**, *7*, 9307–9318. [CrossRef] [PubMed]
6. Yao, Z.; Liao, X.; Gao, K.; Lin, F.; Xu, X.; Shi, X.; Zuo, L.; Liu, F.; Chen, Y.; Jen, A.K.-Y. Dithienopicenocarbazole-Based Acceptors for Efficient Organic Solar Cells with Optoelectronic Response Over 1000 nm and an Extremely Low Energy Loss. *J. Am. Chem. Soc.* **2018**, *140*, 2054–2057. [CrossRef] [PubMed]
7. Zhang, L.; Cole, J.M. Anchoring Groups for Dye-Sensitized Solar Cells. *ACS Appl. Mater. Interfaces* **2015**, *7*, 3427–3455. [CrossRef]
8. Delcamp, J.H.; Yella, A.; Nazeeruddin, M.K.; Grätzel, M. Modulating dye E(S^+/S^*) with efficient heterocyclic nitrogen containing acceptors for DSCs. *Chem. Commun.* **2012**, *48*, 2295–2297. [CrossRef]
9. Reginato, G.; Calamante, M.; Zani, L.; Mordini, A.; Franchi, D. Design and synthesis of organic sensitizers with enhanced anchoring stability in dye-sensitized solar cells. *Pure Appl. Chem.* **2018**, *90*, 363–376. [CrossRef]
10. Liang, M.; Chen, J. Arylamine organic dyes for dye-sensitized solar cells. *Chem. Soc. Rev.* **2013**, *42*, 3453–3488. [CrossRef]
11. Sivanadanam, J.; Ganesan, P.; Madhumitha, R.; Nazeeruddin, M.K.; Rajalingam, R. Effect of π-spacers on the photovoltaic properties of D–π–A based organic dyes. *J. Photochem. Photobiol. A Chem.* **2015**, *299*, 194–202. [CrossRef]
12. Duerto, I.; Sarasa, S.; Barrios, D.; Orduna, J.; Villacampa, B.; Blesa, M.-J. Enhancing the temporal stability of DSSCs with novel vinylpyrimidine anchoring and accepting group. *Dye. Pigm.* **2022**, *203*, 110310. [CrossRef]
13. Masud; Kim, H.K. Redox Shuttle-Based Electrolytes for Dye-Sensitized Solar Cells: Comprehensive Guidance, Recent Progress, and Future Perspective. *ACS Omega* **2023**, *8*, 6139–6163. [CrossRef] [PubMed]
14. Zou, H.; He, B.; Kuang, P.; Yu, J.; Fan, K. Ni_xS_y Nanowalls/Nitrogen-Doped Graphene Foam Is an Efficient Trifunctional Catalyst for Unassisted Artificial Photosynthesis. *Adv. Funct. Mater.* **2018**, *28*, 1706917. [CrossRef]
15. Ma, J.; Li, C.; Yu, F.; Chen, J. 3D Single-Walled Carbon Nanotube/Graphene Aerogels as Pt-Free Transparent Counter Electrodes for High Efficiency Dye-Sensitized Solar Cells. *ChemSusChem* **2014**, *7*, 3304–3311. [CrossRef]
16. Carrera, C.; González-Domínguez, J.M.; Pascual, F.J.; Ansón-Casaos, A.; Benito, A.M.; Maser, W.K.; García-Bordejé, E. Modification of Physicochemical Properties and Boosting Electrical Conductivity of Reduced Graphene Oxide Aerogels by Postsynthesis Treatment. *J. Phys. Chem. C* **2020**, *124*, 13739. [CrossRef]
17. Wu, M.; Lin, X.; Wang, Y.; Wang, L.; Guo, W.; Qi, D.; Peng, X.; Hagfeldt, A.; Grätzel, M.; Ma, T. Economical Pt-Free Catalysts for Counter Electrodes of Dye-Sensitized Solar Cells. *J. Am. Chem. Soc.* **2012**, *134*, 3419–3428. [CrossRef]
18. Hou, S.; Cai, X.; Wu, H.; Yu, X.; Peng, M.; Yan, K.; Zou, D. Nitrogen-doped graphene for dye-sensitized solar cells and the role of nitrogen states in triiodide reduction. *Energy Environ. Sci.* **2013**, *6*, 3356–3362. [CrossRef]
19. Sheng, Z.-H.; Shao, L.; Chen, J.-J.; Bao, W.-J.; Wang, F.-B.; Xia, X.-H. Catalyst-Free Synthesis of Nitrogen-Doped Graphene via Thermal Annealing Graphite Oxide with Melamine and Its Excellent Electrocatalysis. *ACS Nano* **2011**, *5*, 4350–4358. [CrossRef]
20. Cui, Z.; Sheng, W. Thoughts about Choosing a Proper Counter Electrode. *ACS Catal.* **2023**, *13*, 2534–2541. [CrossRef]
21. Rodríguez-Mata, V.; González-Domínguez, J.M.; Benito, A.M.; Maser, W.K.; García-Bordejé, E. Reduced Graphene Oxide Aerogels with Controlled Continuous Microchannels for Environmental Remediation. *ACS Appl. Nano Mater.* **2019**, *2*, 1210–1222. [CrossRef]
22. González-Laínez, M.; Jiménez-Ruiz, M.T.; Martínez de Baroja, N.; Garín, J.; Orduna, J.; Villacampa, B.; Blesa, M.-J. Using functionalized nonlinear optical chromophores to prepare NLO-active polycarbonate films. *Dye. Pigm.* **2015**, *119*, 30–40. [CrossRef]
23. García-Bordejé, E.; Víctor-Román, S.; Sanahuja-Parejo, O.; Benito, A.M.; Maser, W.K. Control of the Microstructure and Surface Chemistry of Graphene Aerogels via PH and Time Manipulation by a Hydrothermal Method. *Nanoscale* **2018**, *10*, 3526–3539. [CrossRef]
24. Schwartz, V.; Fu, W.; Tsai, Y.-T.; Meyer, H.M.; Rondinone, A.J.; Chen, J.; Wu, Z.; Overbury, S.H.; Liang, C. Oxygen-Functionalized Few-Layer Graphene Sheets as Active Catalysts for Oxidative Dehydrogenation Reactions. *ChemSusChem* **2013**, *6*, 840–846. [CrossRef]
25. Che, J.; Shen, L.; Xiao, Y. A new approach to fabricate graphene nanosheets in organic medium: Combination of reduction and dispersion. *J. Mater. Chem.* **2010**, *20*, 1722–1727. [CrossRef]
26. Rodríguez-Mata, V.; Hernández-Ferrer, J.; Carrera, C.; Benito, A.M.; Maser, W.K.; García-Bordejé, E. Towards High-Efficient Microsupercapacitors Based on Reduced Graphene Oxide with Optimized Reduction Degree. *Energy Storage Mater.* **2020**, *25*, 740–749. [CrossRef]
27. Duerto, I.; García-Palacín, M.; Barrios, D.; Garín, J.; Orduna, J.; Villacampa, B.; Blesa, M.-J. A novel σ-linkage to dianchor dyes for efficient dyes sensitized solar cells: 3-methyl-1,1-cyclohexane. *Dye. Pigm.* **2020**, *173*, 107945. [CrossRef]
28. Laschuk, N.O.; Easton, E.B.; Zenkina, O.V. Reducing the resistance for the use of electrochemical impedance spectroscopy analysis in materials chemistry. *RSC Adv.* **2021**, *11*, 27925–27936. [CrossRef] [PubMed]

29. Wu, Y.; Li, G.-D.; Liu, Y.; Yang, L.; Lian, X.; Asefa, T.; Zou, X. Overall Water Splitting Catalyzed Efficiently by an Ultrathin Nanosheet-Built, Hollow Ni_3S_2-Based Electrocatalyst. *Adv. Funct. Mater.* **2016**, *26*, 4839–4847. [CrossRef]
30. Muñoz-García, A.B.; Benesperi, I.; Boschloo, G.; Concepcion, J.J.; Delcamp, J.H.; Gibson, E.A.; Meyer, G.J.; Pavone, M.; Pettersson, H.; Hagfeldt, A.; et al. Dye-sensitized solar cells strike back. *Chem. Soc. Rev.* **2021**, *50*, 12450–12550. [CrossRef] [PubMed]
31. Zambrzycki, M.; Piech, R.; Ruiz Raga, S.; Lira-Cantu, M.; Fraczek-Szczypta, A. Hierarchical carbon nanofibers/carbon nanotubes/NiCo nanocomposites as novel highly effective counter electrode for dye-sensitized solar cells: A structure-electrocatalytic activity relationship study. *Carbon* **2023**, *203*, 97–110. [CrossRef]
32. Xi, J.-Y.; Jia, R.; Li, W.; Wang, J.; Bai, F.-Q.; Eglitis, R.I.; Zhang, H.-X. How does graphene enhance the photoelectric conversion efficiency of dye sensitized solar cells? An insight from a theoretical perspective. *J. Mater. Chem. A* **2019**, *7*, 2730–2740. [CrossRef]
33. Yang, R.-Y.; Chen, H.-Y.; Lai, F.-D. Performance Degradation of Dye-Sensitized Solar Cells Induced by Electrolytes. *Adv. Mater. Sci. Eng.* **2012**, *2012*, 902146. [CrossRef]
34. Lai, S.C.; Connor, K.N.P.; Ke, L. Degradation Mechanisms and Electron Kinetics Analysis in Aging Dye Sensitized Solar Cell Using Electrochemical Impedance Spectroscopy. *J. Electrochem. Soc.* **2011**, *158*, H1193. [CrossRef]